JOURNAL OF PROPULSION AND POWER
Vol. 31, No. 4, July–August 2015

Development and Testing of Hall Thruster with Flexible Magnetic Field Configuration

S. Mazouffre,* G. Bourgeois,† and J. Vaudolon‡
Centre National de la Recherche Scientifique, 45071 Orléans, France
L. Garrigues§
Université de Toulouse, F-31062 Toulouse Cedex 9, France
C. Hénaux,¶ D. Harribey,** R. Vilamot,†† and A. Rossi‡‡
Université de Toulouse, F-31071 Toulouse Cedex 7, France
and
S. Zurbach§§ and D. Le Méhauté¶¶
Snecma, 27208 Vernon, France

DOI: 10.2514/1.B35417

The magnetic field at the origin of the electron confinement in a Hall thruster is established by means of an assembly composed of coils or magnets and a circuit that guides the flux. The standard magnetic architecture, however, suffers from a lack of flexibility as its main purpose is to generate a well-defined topology that warrants a high and stable performance level. This contribution reports on a thruster with an unconventional magnetic circuit that allows covering a broad range of magnetic field topologies. Compared with a classical magnetic circuit, the proposed circuit is especially designed to control in an independent manner all the characteristic parameters of a magnetic topology. The new magnetic structure is mounted in a thruster prototype based on the PPS®1350-ML Hall thruster architecture. The prototype is named PPS-Flex. First, the design and construction of this original magnetic assembly are presented together with functioning of the control interface. Second, the flexibility is illustrated through several examples of achievable magnetic field configurations. Third, experimental results obtained during test campaigns of the PPS-Flex thruster fed with xenon as propellant gas are described and discussed.

Nomenclature

$\boldsymbol{B}$	=	magnetic field vector, G
B_x	=	magnetic field axial component, G
B_y	=	magnetic field radial component, G
I_d	=	discharge current, A
I_{sp}	=	specific impulse, s
T	=	thrust, N
U_d	=	discharge voltage, V
x	=	axial coordinate, m
y	=	radial coordinate, m
α	=	propellant usage
η	=	total efficiency
θ	=	divergence half-angle, deg
Φ_a	=	anode mass flow rate, mg/s

Received 8 April 2014; revision received 8 January 2015; accepted for publication 8 January 2015; published online 26 March 2015.

*Research Scientist, Institut de Combustion Aérothermique Réactivité et Environnement, 1 C Avenue de la Recherche Scientifique; stephane.mazouffre@cnrs-orleans.fr.

†Engineer, Institut de Combustion Aérothermique Réactivité et Environnement, 1 C Avenue de la Recherche Scientifique; currently Phasics; bourgeois@phasics.fr.

‡Ph.D. Candidate, Institut de Combustion Aérothermique Réactivité et Environnement, 1 C Avenue de la Recherche Scientifique; julien.vaudolon@cnrs-orleans.fr.

§Research Scientist, Laboratoire Plasma et Conversion d'Energie, UPS, INPT Toulouse 118, route de Narbonne; also CNRS, LAPLACE, F-31062 Toulouse, France; laurent.garrigues@laplace.univ-tlse.fr.

¶Associate Professor, Institut National Polytechnique de Toulouse; carole.henaux@laplace.univ-tlse.fr.

**Currently Engineer, CNRS; dominique.harribey@laplace.univ-tlse.fr.

††Engineer, Laboratoire Plasma et Conversion d'Energie, UPS, INPT Toulouse, 2 rue Charles Camichel; currently Liebherr; raphael.vilamot@liebherr.fr.

‡‡Ph.D. Candidate, Laboratoire Plasma et Conversion d'Energie, UPS, INPT Toulouse, 2 rue Charles Camichel; alberto.rossi@laplace.univ-tlse.fr.

§§Engineer, Safran Group, Space Engines Division, Plasma Propulsion Unit, Forêt de Vernon, BP 802; stephan.zurbach@scnecma.fr.

¶¶Engineer, Safran Group, Space Engines Division Plasma Propulsion Unit, Forêt de Vernon, BP 802; david.lemehaute@snecma.fr.

I. Introduction

A HALL thruster (HT) is an efficient ion accelerator dedicated to spacecraft propulsion [1–3]. The principle of a HT is based on crossed magnetic and electric fields to ionize and accelerate a propellant gas. Hall thrusters are currently employed for geostationary communication satellites orbit correction and station keeping. The next generation of Hall thrusters will be devoted to maneuvers and missions that require a higher thrust level like satellite orbit topping and orbit transfer as well as solar system exploration.

A Hall thruster is a magnetized low-pressure dc discharge maintained between an external cathode and an anode [4,5]. The anode, which often serves as gas injector, is located at the upstream end of a coaxial annular dielectric channel that confines the discharge. Xenon is used as a propellant gas for its specific properties in terms of atomic mass and ionization energy. A set of solenoids or permanent magnets provides a radially directed magnetic field, the strength of which is maximum in the vicinity of the channel exhaust. The magnetic field is chosen strong enough to make the electron Larmor radius much smaller than the thruster discharge chamber sizes but weak enough not to disturb ion trajectories. The electric potential drop is mostly concentrated in the final section of the channel owing to the high electron resistivity. The resulting axial electric field drives a large electron azimuthal drift, the Hall current, which is responsible for the efficient ionization of the gas. The electric field also accelerates ions out of the channel, which generates thrust and specific impulse. The ion beam is neutralized by a fraction of electrons emitted from the cathode. Modern Hall thrusters deliver a thrust-to-power ratio in excess of 50 mN/kW, far above what is produced by gridded ion engines [6], with an efficiency around 60%.

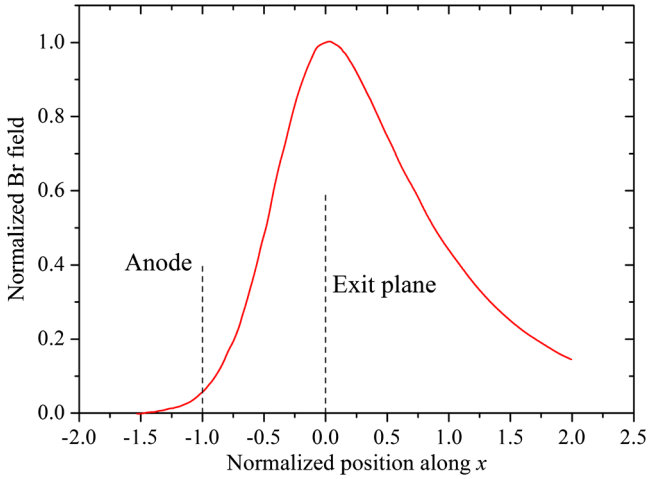

Fig. 1 Distribution of the radial magnetic field strength (Br) along the channel axis for a conventional Hall thruster magnetic design (reference profile in this work).

The specific impulse is nevertheless moderate with a typical value of 2500 s under normal operating conditions.

The magnetic structure of a conventional HT comprises two main elements: a series of coils or magnets to produce the magnetic flux and a conducting circuit to guide the flux and to shape the $\boldsymbol{B}$ field. The circuit, which is made of a ferromagnetic material like iron or an iron-cobalt alloy, has typically two pole pieces. Magnetic screens can be added if necessary. The usual configuration is composed of one central coil and coils around the outer channel wall. The two parts are not necessarily electrically connected in series. With a standard configuration, the $\boldsymbol{B}$ field is the highest at the channel exhaust with a positive (negative) gradient inside (outside), the channel when following the ion flow direction. An example of $\boldsymbol{B}$ field distribution along the channel axis is shown in Fig. 1. The magnetic field lines form an ion lens that is symmetrical about the channel axis [4,7]. The lens tends to focus the ions out of the channel into a well-defined beam. As previously explained, the magnetic field plays a major role in a Hall thruster as it controls to a large extent both the ionization of the neutral gas and the acceleration of the ions. Besides, the magnetic field topology influences the charged-particle flux to the channel walls, with direct consequences on the thermal load and the erosion level. Finally, the magnetic field lines curvature and angle influence the ion beam properties. Therefore, it appears necessary to optimize the magnetic field topology in order to reach a high performance level and a long operational lifetime.

The influence of the magnetic field topology upon the performances and the discharge characteristics of a Hall thruster has been studied in the past using a conventional magnetic architecture from an experimental as well as a numerical point of view; see, e.g., [8–12]. For instance, Hofer et al. extensively examined the influence of the magnetic field topology on the performances of the 5 kW-class NASA-173M v2 Hall thruster [8,9]. For that purpose, they added two trim coils to the original magnetic structure in order to obtain additional control of the magnetic field topology. A first trim coil was placed behind the anode to increase the $\boldsymbol{B}$ field gradient inside the channel. A second trim coil was located outside the channel. When energized, the magnetic field topology downstream of the thruster channel exit plane changes, especially the inclination of the ion lens. Despite the use of additional trim coils, modifying one characteristic parameter of the magnetic topology induces a change in other characteristics. In other words, the use of a standard magnetic circuit does not allow varying one parameter while keeping all others fixed. This aspect makes any precise study on the $\boldsymbol{B}$ field impact very complicated.

This paper presents a new and versatile magnetic structure, which is free from the physical constraints of an usual design. The magnetic structure has been mounted in a dedicated thruster based on the PPS®1350-ML architecture. The prototype is named PPS-Flex, as it appears to be extremely flexible in terms of magnetic field configurations. The objectives of the research program involving the PPS-Flex thruster are manyfold, namely, to better understand the influence of the magnetic field, to investigate unexplored operating conditions, and to optimize the $\boldsymbol{B}$ field topology for high-efficiency operation and long lifetime. Section II describes in detail the design of the new magnetic architecture and the construction of the PPS-Flex thruster. It is also devoted to the interfaces for the magnetic field definition and the coil power unit control. Section III gives several magnetic topologies that can be realized using this new magnetic circuit. Operation of the PPS-Flex thruster with xenon as well as performance measurements for different magnetic topologies are described in Sec. IV. Section V demonstrates the possibility to create configurations of the magnetic shielding type. Finally, conclusions as well as prospects are drawn in Sec. VI.

II. Magnetic Assembly of PPS-Flex Hall Thruster

A. Specifications

Before the building of a dedicated device for a thorough investigation of the influence of the magnetic topology on Hall thruster performances, a list of prerequisites was established. First, in terms of design, the magnetic structure must be compatible with the geometry of the channel of the PPS®1350-ML Hall thruster. Second, the device must be able to reproduce the magnetic field map of the PPS®1350-ML thruster in normal operating conditions, which is the reference configuration for this work. The on-axis profile of the corresponding $\boldsymbol{B}$ field radial component is given in Fig. 1. Those two points were motivated by the fact that a large amount of data about the PPS®1350-ML thruster operation have been collected over the years. Finally, the proposed magnetic structure must allow controlling several magnetic parameters simultaneously and in an independent manner, therefore offering a large set of degrees of freedom. This essential feature makes the PPS-Flex thruster unique. The magnetic parameters to be adjusted are 1) the magnetic field gradients inside and outside the channel, 2) the strength of the field, 3) the position of the maximum of the magnetic field amplitude, 4) the width of the profile, 5) the curvature of the lines, 6) the inclination of the lens, and 7) the amplitude of the field near the anode.

In addition, one must be able to create a zero-magnetic field region near the anode and to control its location.

B. Unconventional Magnetic Structure

To drastically increase the set of possible magnetic field configurations, one solution consists of increasing the number of independent magnetic flux sources and ferromagnetic parts. Using the knowledge of some of the authors in the field of magnetic actuators with slotted armature, the final design of the PPS-Flex magnetic circuit combines elementary parts composed of a coil wrapped around a ferromagnetic bore and inserted in between two ferromagnetic disks, as shown in Fig. 2 [13]. Each component is dedicated to one specific function. The coil generates the magnetic field. The magnetic bore concentrates the magnetic field. The ferromagnetic disks conduct the flux lines to obtain the desired topology inside and outside the channel. The various materials for the building of the magnetic structure have been selected, taking into account constraints like thermal load, weight, and cost [14]. Coils are made of cerafil, and all ferromagnetic parts are made of pure iron. Electrical insulation is realized with ceramic compounds like alumina and MACOR®. Compared with the conventional PPS®1350-ML thruster, both the channel and magnetic assembly have been lengthened. As can be seen in Fig. 2, an external conic part has been added. The coils and the ferromagnetic parts that make this last section are necessary to control the magnetic field gradients outside the channel. To protect those coils from the thermal heat flux and from ion bombardment, the additional section is shielded with a ceramic piece. The conic shape is such that the ceramic screen has a limited interaction with the plasma downstream the annular channel. Notice that the additional section can be removed. In that case, the

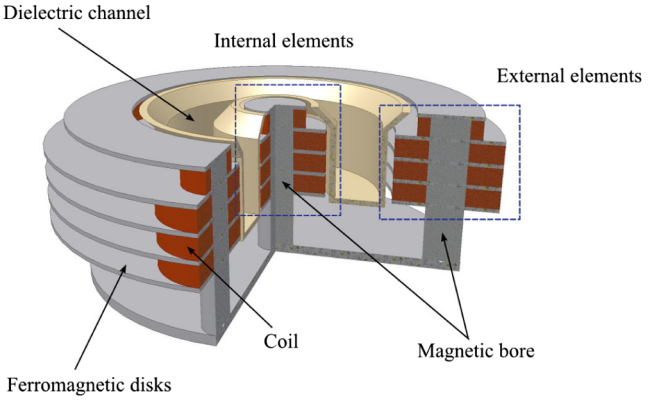

Fig. 2 Schematic of the PPS-Flex magnetic assembly showing the coils and the ferromagnetic guides. Note the two back coils are not depicted. The dielectric channel is also shown.

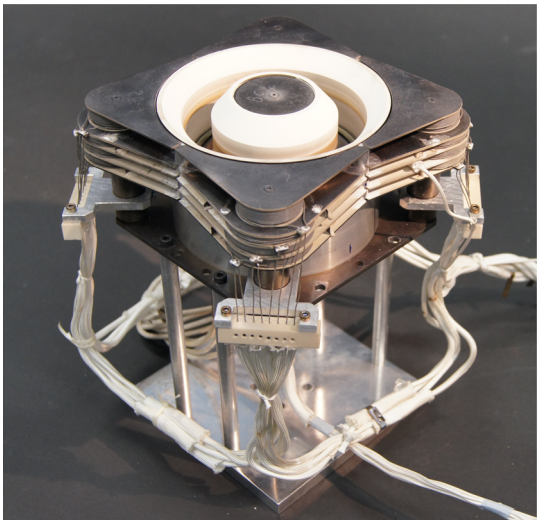

Fig. 3 Photograph of the PPS-Flex Hall thruster without the external cathode.

PPS-Flex channel becomes similar to the one of the PPS®1350-ML, however, at the expense of magnetic flexibility.

To obtain homogeneity in the azimuthal direction, the perfect solution consists of designing an axisymmetric magnetic circuit with an external coil wrapped around the channel. This arrangement is not satisfying for thermal and practical points of view. On the one hand, the coil that encircles the ceramic channel forms a thermal barrier for the energy flux produced by the plasma. On the other hand, this coil configuration does not make easy the experimental characterization of the discharge with wall probes and laser spectroscopy techniques. As a consequence, the magnetic circuit final design rests on a set of external coils distributed in a symmetric way around the external circumference of the channel. The magnetic circuit of the PPS-Flex is divided into four stages, as illustrated in Fig. 2. Four external coils located around the outer wall of the channel and one internal coil wrapped around the central core constitute one stage. As one can see, each stage is powered independently. The stage number results from a tradeoff between performances, dimensions, complexity, weight, and cost. Each stage provides degrees of freedom for controlling the magnetic field topology. When the stage number increases, the number of achievable magnetic field maps increases as well. So the natural tendency would be to opt for a great number of stages. However, increasing the number of stages while keeping unchanged the length of the magnetic structure implies a reduction of the coil thickness and the gap between the ferromagnetic disks at the same time. Furthermore, when the gap between the disks is narrow, the magnetic field lines can be short circuited without penetrating inside the channel anymore. For these reasons, the number of coils must be limited. The appropriate number of coils, as well as the geometry of the magnetic circuit, was determined using an optimization procedure. The chosen approach is parametric and based on computer simulations [13]. Several magnetic configurations were modeled using the Finite Element Method Magnetics (FEMM) software [15]. The approach was to gradually increase the level of complexity, i.e., the number of components, from one configuration to the next. The magnetic field topology was subsequently computed using a MATLAB® program based on a superposition property that assumes the total magnetic field to be a linear combination of the fields produced by individual, separately powered coils. The optimization procedure led to the design of the four-stage structure previously described [13,14].

C. PPS-Flex Thruster

The total number of coils for the PPS-Flex thruster is finally 22. The magnetic assembly includes the 20 coils previously described and shown in Fig. 2. In addition, two complementary coils are located behind the back wall of the channel. They allow better controlling the zero-field region near the anode as well as the internal gradients. With this configuration, the number of degrees of freedom is 10: four internal coils; four external stages, each with four coils connected in series; and the two back coils. The PPS-Flex operation therefore requires independently controlling ten power supplies just for the $\boldsymbol{B}$ field generation.

A photograph of the PPS-Flex prototype is shown in Fig. 3 without the external hollow cathode. The conic ceramic screen, the channel, and the four outer magnetic stages are clearly visible. Figure 4 gives an example of a magnetic field topology that can be obtained with the PPS-Flex prototype. This classical topology is close to the magnetic configuration of the PPS®1350-ML Hall thruster under normal operating conditions, which is the reference topology for this study. The corresponding profile of the $\boldsymbol{B}$ field along the channel centerline is shown in Fig. 1. Leaks of the magnetic flux in between the ferromagnetic disks are visible in Fig. 4.

D. Control of Magnetic Field

In view of the complexity of the magnetic circuit, a sophisticated control interface is necessary to properly operate the PPS-Flex

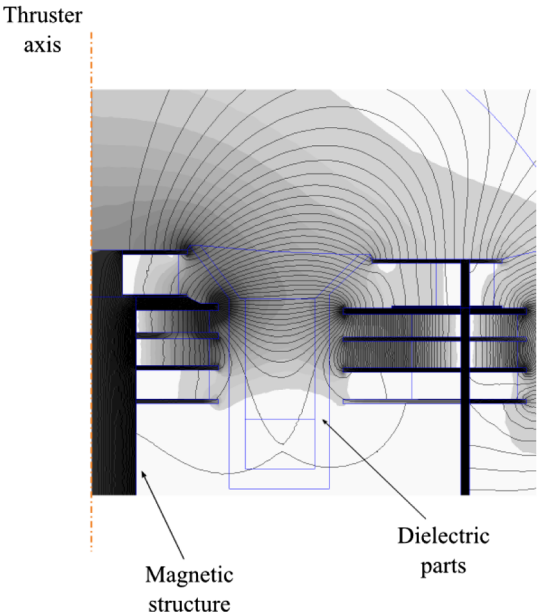

Fig. 4 Reference magnetic field topology of the PPS-Flex thruster (numerical simulation). The ferromagnetic disks, the channel, and the conic shield are shown. The gray color scale indicates the $\boldsymbol{B}$ field magnitude.

thruster. Three main requirements have been identified. The user must be able to easily define a magnetic field topology from a small number of parameters. A dedicated software must compute and optimize the current in each coil afterward. Finally, a program must drive the coil power supplies and verify functioning of the whole magnetic assembly. The process is divided in two parts. A first display permits the definition of the magnetic topology in the channel, for computation of the necessary currents in each coil and for visualization of the resulting magnetic field map. A second display permits the manual/automatic control of the coil power supplies. Note that currently the two coils placed behind the channel are separately powered.

As a starting point, a radial component and an axial component of the magnetic field must be defined in a cross-section of the thruster channel. The coil currents are then obtained by interpolation from a set of reference magnetic topologies. The FEMM software has been used to numerically compute the magnetic field generated by each stage of the magnetic circuit for a unitary current (1 A) in all coils. Assuming the magnetic circuit is not saturated, the total magnetic field in the channel is then the sum of the elementary magnetic fields. An algorithm is used to interpolate the field and retrieve the proper currents in each coil under the assumption of magnetic linearity. An optimization process is applied with the minimization of currents as a criterion. The magnetic field that results from the optimization process is visualized in real time. The reverse operation is also possible: the user may set the current in each coil and automatically view the resulting magnetic field topology. Detailed information about the calculation and optimization procedures can be found in [13].

III. Magnetic Flexibility

This section illustrates the capability of the PPS-Flex magnetic circuit to generate various and accurate magnetic field topologies by independently controlling the ***B*** field parameters. All magnetic field distributions shown in the next figures correspond to the numerical outcome of the interface. Measurements of several simulated ***B*** field topologies have been carried out with a three-dimensional Gaussmeter equipped with a three-axis magnetic probe [16]. In all cases, there is a satisfactory agreement between the measured and the calculated maps. As an example, Fig. 5 shows a comparison between a measured and a computed map of the magnetic field magniture for a standard configuration. The difference between measurement and simulation is better illustrated in Fig. 6, which presents the magnetic field distribution along the channel axis for the configuration of Fig. 5. The graph also indicates the small gap between a linear and a nonlinear computer simulation. Note that in the following figures the third profile always corresponds to the reference radial magnetic field profile; see Fig. 1.

Figure 7 shows the change in the positive and negative gradients of the magnetic field along the channel centerline. Only the radial component B_y of the field is considered here. The peak of the magnetic field magnitude is located at the channel exit plane. The axial coordinate x is normalized to the length of the channel. The $x = 0$ position corresponds to the end of the straight section of the channel. The anode is located at $x = -1$. The on-axis B_y distributions plotted in Fig. 7 demonstrate that it is possible to control independently the gradient inside and outside the channel without modifying the magnitude and position of the magnetic field. Moreover, varying the dc current flowing into the coils allows significantly modifying the magnetic field gradient. In Fig. 7, the change reaches 25% upstream and 38% downstream of the channel exit plane, respectively. To not modify the width of the axial distribution when varying the gradients, it is possible to fix the inflection points of the magnetic profile.

One can also vary the magnetic field strength over a relatively broad range, as illustrated in Fig. 8. With the current version of the

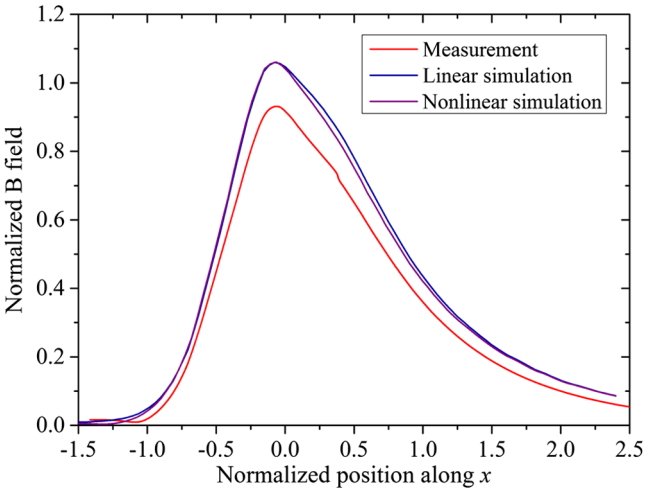

Fig. 6 Distributon of the normalized magnitude of the magnetic field along the channel axis (configuration of Fig. 5); comparison between measurement, linear simulation and nonlinear simulation.

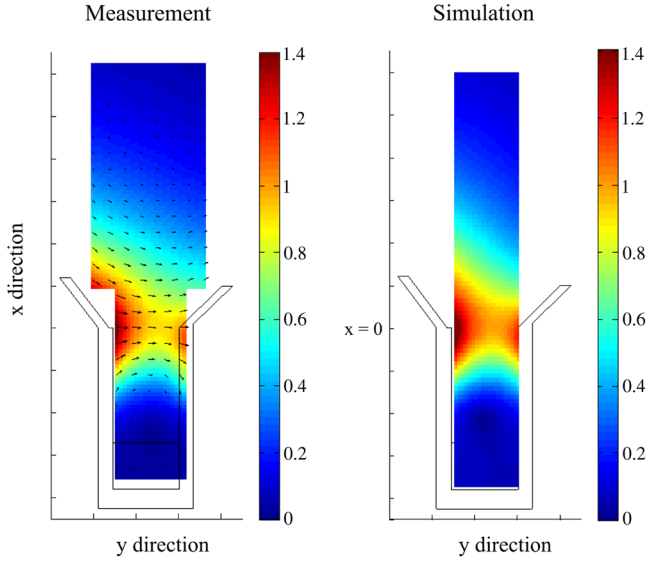

Fig. 5 Contour plot of the normalized magnitude of the magnetic field from a measurement with a three-dimensional Gaussmeter and a linear computer simulation. The coil current is the same in the two cases.

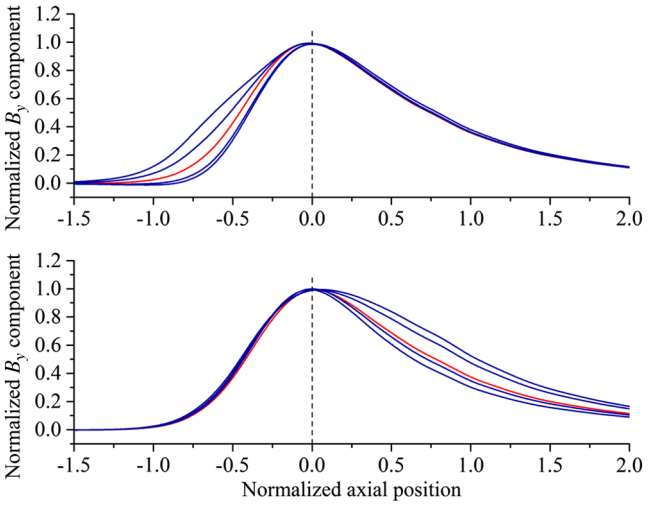

Fig. 7 Distribution of the radial component of the magnetic field B_y along the PPS-Flex channel axis. Top: Change in the gradient inside the channel. Bottom: Change outside the channel. The $x = 0$ coordinate corresponds to the end of the straight section of the channel. The anode is placed at $x = -1$.

PPS-Flex prototype, the highest value of the magnetic field can be change by ±30% from the reference profile. The position of the peak of the B_y axial distribution is not affected when varying the magnitude; however, as can be seen in Fig. 8, the gradients are obviously changed. The PPS-Flex thruster of course allows modifying both the magnitude and the gradients if necessary. The entire magnetic field distribution can also be shifted, as shown in Fig. 9. The peak of the B_y profile can then be located either inside or outside the channel. A last example concerns the inclination of the magnetic field lines. By modifying the strength of the axial magnetic field component, one is able to change the inclination of the magnetic field lines; see Fig. 10. With the PPS-Flex thruster, the inclination angle can be adjusted from −6 to 12 deg, a 0 deg angle corresponding to a line perpendicular to the channel axis. The line inclination has an influence upon the inclination of the electrostatic ion lens, which, in turn, affects the ion beam divergence.

Other magnetic parameters can naturally be varied, like the curvature of the flux lines, the creation of a zero-magnetic field region near the anode as well as the fine positioning of this region, the width of the axial distribution, and magnetic mirror effects. Examples and a discussion can be found in [13] and [16].

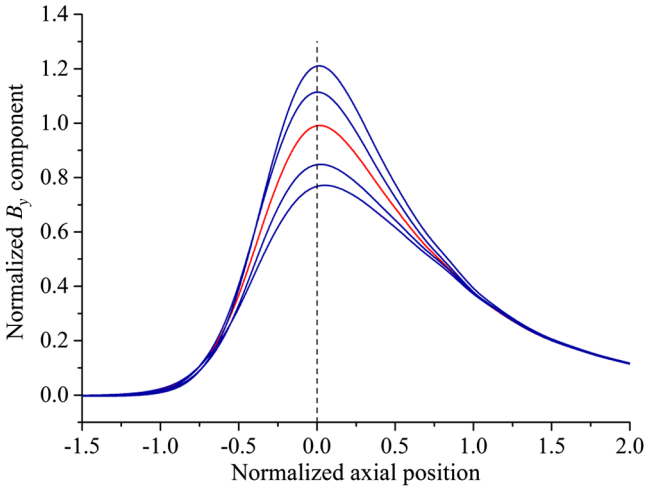

Fig. 8 Change in the magnitue of the distribution of B_y along the PPS-Flex channel axis.

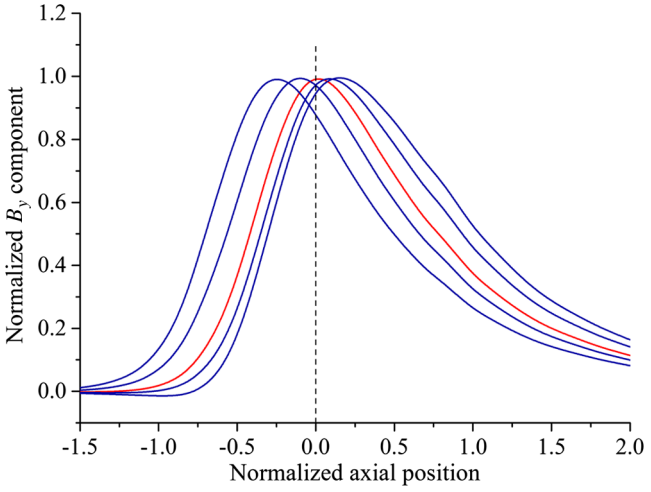

Fig. 9 Shifting of the distribution of B_y along the PPS-Flex channel axis.

IV. Examples of Relationship Between Magnetic Configuration and Performances

Series of test campaigns have been performed during the past two years in various vacuum test chambers with the PPS-Flex thruster. The first experiments were of course dedicated to testing the prototype and verification of the magnetic flexibility during operation. The objective of the measurement campaigns was to investigate in depth the interconnection between the magnetic field topology, the performance, and the discharge properties. More than 100 ***B*** field configurations have been examined to date. This section gives a few examples of tested magnetic field configurations with associated performances to illustrate the PPS-Flex potential under real conditions.

The PPS-Flex thruster was fired with xenon as a propellant gas. The thruster was equipped with BN-SiO_2 walls for the straight channel as well as the conic section. A cold hollow cathode was used as a beam neutralizer. The thruster was operated at a fixed discharge current value of 4.28 A, which means the xenon mass flow rate automatically adjusted itself. The discharge voltage was varied between 200 and 350 V. The input power never exceeded 1500 W to limit the thermal load. The vacuum chamber background gas pressure was typically 2×10^{-5} mbar-Xe. The thruster was mounted onto a calibrated thrust balance to determine the thrust level and the specific impulse. The thrust error bar was ±1.5 mN for the range of interest. A 70-cm-radius rotating arm equipped with 15 Faraday probes was used to measure the ion current density profile in the ion beam far field. The total ion current was computed assuming a cylindrical symmetry of the beam after correction of the current profile for charge-exchange collisions [17,18]. The divergence the half-angle

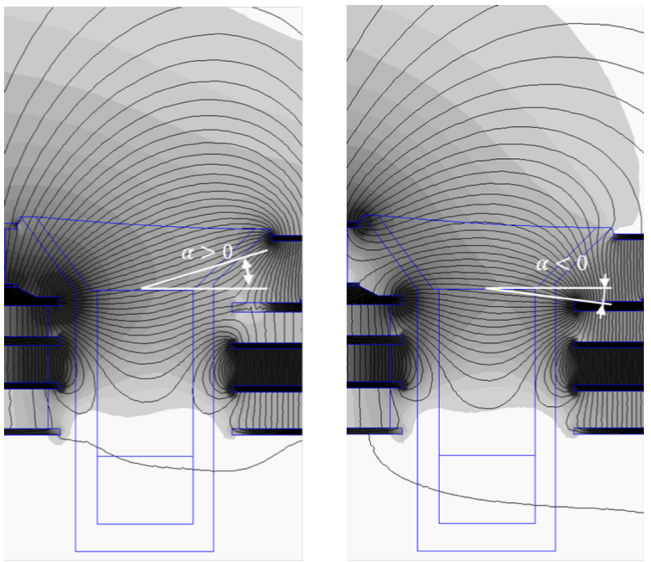

Fig. 10 Inclination of the magnetic field lines.

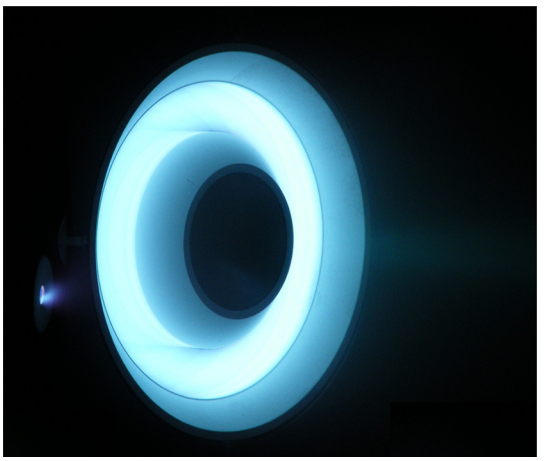

Fig. 11 Photograph of the PPS-Flex thruster in operation with xenon as a propellant gas for the reference magnetic field topology. The external cathode is placed on the left.

Table 1 The 13 selected PPS-Flex magnetic configurations

PPS-Flex magnetic configurations			
Number	Magnetic characteristic	Number	Magnetic characteristic
1	PPS®1350-ML (reference)	5	Shift of B inside the channel
2	SPT100	6–10	Positive and negative lens inclination
3, 4	Steep gradient inside the channel	11–13	Moving of the zero B field region

from the thruster centerline θ corresponds here to the half-angle over which the ion current density represents 90% of the total ion current. A photograph of the PPS-Flex thruster in operation with the reference magnetic topology is shown in Fig. 11. The conic part of the channel can clearly be seen. The plasma discharge is confined into the straight part of the annular channel.

The PPS-Flex capability of generating different magnetic field configurations is here exemplified through 13 magnetic topologies, which are summarized in Table 1. The latter also gives the identification number for the remainder of the paper. The topologies include standard configurations such as the PPS®1350-ML-type and SPT100-type $\boldsymbol{B}$ field. For configurations 3 and 4, the positive $\boldsymbol{B}$ field gradient inside the channel is increased compared to 1 and 2 by moving downstream of the zero-field region. The maximum of the radial magnetic field component B_r is located inside for the configuration 5, all other parameters being unchanged. The lens inclination at the straight channel exit plane for configurations 6–10 are 0, 6, −6, −19, and 19 deg, respectively. Here, a negative angle corresponds to a lens directed toward the thruster centerline. Configuration 11 is similar to 5, except that a zero-field region is created downstream of the thruster exit plane. Configuration 12 has two zero-field regions: one inside and one outside the channel. Configuration 13 corresponds to 12 with a lower magnetic field amplitude. The 22 coils together with the 10 power units are needed to generate the aforementioned family of topologies.

The measured thrust level is given in Fig. 12 for the 13 magnetic configurations previously described. Figure 12 also displays the total efficiency η, which accounts for the cathode gas flow rate. Measurements were carried out for a discharge voltage of 250 V. The power furnished to the discharge was 1070 W. Configurations labeled 4, 12, and 13 were not stable for this set of operating conditions. Current oscillations were large, and the discharge switched off after a short time span. The highest thrust level and the largest efficiency were reached for the first three configurations, which can be considered standard. The magnetic configuration labeled 7, which exhibited a negative lens inclination, led to relatively good performances. However, because of the inclination angle, the temperature of the inner channel ceramic wall was high, which means the erosion rate was certainly large with direct consequence on the thruster lifetime. The reference configuration labeled 1 in fact gave values for the discharge current, the thrust, the specific impulse, and the efficiency very close to the ones obtained with the PPS®1350-ML Hall thruster whatever the applied voltage. First, it indicated the PPS-Flex magnetic circuit can accurately reproduce the normal PPS®1350-ML magnetic field map. Second, it showed the weak effect of the additional conic section on the discharge and plume properties. As can be seen in Fig. 12, the PPS®1350-type magnetic configuration 1 produced performances above the SPT100-type configuration 2. However, the order depended on the background pressure and on the cathode electrical wiring.

Figure 13 shows the anode mass flow rate in xenon Φ_a necessary to maintain the discharge current at 4.28 A for the 13 magnetic configurations of the PPS-Flex. In that case, the mass flow rate gave information about the ionization efficiency. Φ_a was relatively high for the PPS®1350-ML $\boldsymbol{B}$ field topology; however, it was below the value measured with the SPT100-type topology. The lowest xenon mass flow rate was obtained with the configuration labeled 5, which means when moving upstream the peak of the magnetic field axial profile. But the thrust and the efficiency were low with this configuration, as shown in Fig. 12, due to an increase in the losses at walls.

The set of experimental data is summarized in Table 2 for a discharge voltage of 250 V and a current discharge of 4.28 A. The specific impulse is computed from the thrust level. The quantity α is the ionization efficiency, or propellant usage, and θ is the beam divergence half-angle. The largest specific impulse was reached with the PPS®1350-ML configuration, which also gave a low beam divergence. The propellant usage was a bit improved when the gradient inside the cavity was steeper.

V. Magnetic-Shielding-Type Configurations

The main drawback of conventional HTs is their relatively short operational lifetime, at least compared to gridded ion engines. The

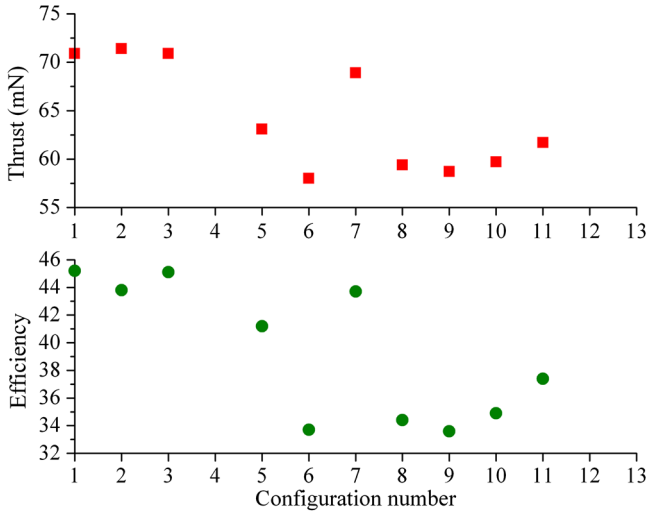

Fig. 12 Thrust and total efficiency of the PPS-Flex thruster at 250 V applied voltage and 1070 W input power for various magnetic configurations (see Table 1).

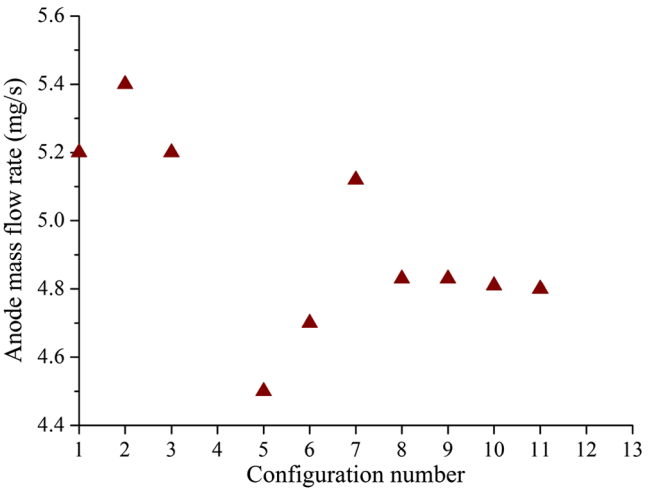

Fig. 13 Xenon anode mass flow rate at 250 V applied voltage needed to maintain the discharge current at 4.28 A for various magnetic configurations (see Table 1).

Table 2 Performance data of the PPS-Flex thruster for several magnetic configurations

Experimental data: $U_d = 250$ V and $I_d = 4.28$ A						
Configuration number	T, mN	Φ_a, mg/s	α	η	I_{sp}	θ, deg
1	70.9	5.2	0.72	0.45	1446	36.7
2	71.4	5.4	0.71	0.44	1379	35.5
3	70.9	5.2	0.74	0.45	1367	35.6
4	— —	— —	— —	— —	— —	— —
5	63.1	4.5	— —	0.41	1410	— —
6	58.0	4.7	0.57	0.34	1258	40.5
7	68.9	5.1	0.73	0.44	1371	38.6
8	59.4	4.85	0.59	0.34	1254	39.0
9	58.7	4.85	0.61	0.33	1237	40.7
10	59.7	4.8	0.58	0.35	1267	40.1
11	61.7	4.8	0.65	0.37	1310	39.8
12	— —	— —	— —	— —	— —	— —
13	— —	— —	— —	— —	— —	— —

primary factor that limits the lifetime is the erosion of the dielectric annular channel walls due to high-energy ion bombardment. Besides, plasma/wall interaction generates power losses and thermal stress on the structure components. The large particle flux toward the walls is a direct consequence of the magnetic field topology. As explained in the Introduction, in a HT, the accelerating electric field originates in a decrease of the electron mobility in the region of a strong $\boldsymbol{B}$ field. An efficient electron trapping necessitates a radial magnetic field of which the lines intersect the walls, as can be seen in Fig. 4. Recently, an original approach to significantly reduce the erosion rate, hence elongating the thruster lifetime, has been proposed and validated. This approach is termed magnetic shielding (MS) [19–21]. MS consists of preventing the magnetic field lines from crossing the walls in the acceleration region. Instead, the lines must stay parallel to the wall of the downstream channel section, and they must extend to the anode region to capture cold electrons. Such a topology strongly reduces the radial electric field component magnitude in the final section of the channel, thereby decreasing wall material sputtering. MS-type configurations can be achieved with the PPS-Flex Hall thruster.

Figure 14 shows a photograph of the PPS-Flex thruster fired at 250 V and a 3.5 mg/s xenon anode flow rate in the MS configuration. In that case, the plasma forms a ring in the conical section. The ionization and acceleration zones are certainly shifted downstream of the exit plane, which explains the low light intensity inside the straight part of the channel. Moreover, the plasma is detached from the walls as illustrated by the fact that there is a dark area in the conical part between the plasma and the surface. This picture must be compared to Fig. 11, in which the PPS-Flex thruster is fired in a standard unshielded magnetic configuration; i.e., the force lines are perpendicular to the BN-SiO_2 walls at the channel exhaust. The plasma is then concentrated inside the straight section of the channel where it interacts with the walls. In Fig. 14, the ion beam appears less sharp. It results from a low magnetic field intensity (90 G) due to the coil current limit set for this configuration. With this MS topology, the PPS-Flex thrust level is about 20% less than that obtained with a standard configuration under similar conditions, but the $\boldsymbol{B}$ field is weak, and the MS topology is not optimized [22,23].

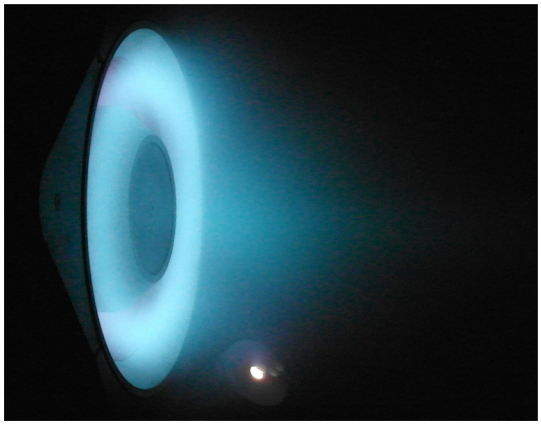

Fig. 14 Photograph of the PPS-Flex thruster operating with xenon at 250 V discharge voltage and 3.5 mg/s anode mass flow rate in the magnetic-shielding-type configuration with the lines parallel to the walls both in the conical section and in the upstream end of the channel.

VI. Conclusions

The recently developed 1.5 kW class PPS-Flex Hall thruster has been tested and validated. The PPS-Flex is a unique Hall thruster prototype because it offers the possibility of separately controlling all magnetic parameters. The number of magnetic field topologies that can be achieved is vast. Configurations range from the classical SPT100 to the magnetic shielding and mode without a wall [23] and include tilted lenses and zero-field maps. A large amount of $\boldsymbol{B}$ field topologies has been characterized over an input power range from 500 W up to 1.8 kW in terms of related performances and discharge properties. Experiments are still ongoing with new sets of magnetic configurations.

The objectives of the works involving the PPS-Flex are twofold: 1) to improve the performances of standard Hall thrusters and 2) to validate topologies for stable operation at high voltage (high I_{sp}) and over a long period of time. To achieve the goals, a first step consists of acquiring macroscopic quantities like thrust, discharge current, and beam divergence for a large number of magnetic configurations and a broad range of operating parameters. The data set allows selection between topologies. It also brings original information about the effect of the magnetic field distribution. For instance, this study reveals the lens angle should stay small, gradients should be moderate, and the maximum should not be moved deep inside the channel. In addition, this work indicates classical magnetic field topologies offer a high level of performance. But it also indicates margins of improvement do exist. A second, more fundamental, step is, however, necessary. Advanced diagnostic techniques such as laser-induced fluorescence spectroscopy and coherent Thomson scattering must be combined with modeling and numerical simulations to capture the complex relationship between the magnetic field, the discharge properties, and the overall performances.

Acknowledgments

This study was financially supported by the French Space Agency (Centre National d'Etudes Spatiales). A. Rossi is a Ph.D. candidate with a Centre National d'Etudes Spatiales/Snecma grant. R. Vilamot benefitted from a Centre National d'Etudes Spatiales/Snecma grant. J. Vaudolon benefitted from a Centre National d'Etudes Spatiales/Snecma Ph.D. grant. G. Bourgeois benefitted from a CIFRE Ph.D. grant. This work was performed within a French joint research program between the LAPLACE laboratory, the ICARE laboratory, and the SNECMA company.

References

[1] Frisbee, R. H., "Advanced Space Propulsion for the 21st Century," *Journal of Propulsion Power*, Vol. 19, No. 6, 2003, pp. 1129–1154. doi:10.2514/2.6948

[2] Goebel, D. M., and Katz, I., *Fundamentals of Electric Propulsion*, Wiley, Hoboken, NJ, 2008, Chaps. 7–9.

[3] Ahedo, E., "Plasmas for Space Propulsion," *Plasma Physics Controlled Fusion*, Vol. 53, No. 12, 2001, Paper 124037. doi:10.1088/0741-3335/53/12/124037

[4] Zhurin, V. V., Kaufmann, H. R., and Robinson, R. S., "Physics of Closed Drift Thrusters," *Plasma Sources Science and Technology*, Vol. 8, No. 1, 1999, pp. R1–R20. doi:10.1088/0963-0252/8/1/021

[5] Dannenmayer, K., and Mazouffre, S., "Elementary Scaling Relations for Hall Effect Thrusters," *Journal of Propulsion Power*, Vol. 27, No. 1, 2011, pp. 236–245. doi:10.2514/1.48382

[6] Mazouffre, S., and Lejeune, A., "High Power Electric Propulsion for Robotic Exploration of Our Solar System," *Proceedings of 1st International Conference on Space Access*, Astech, Paris, 2011, Paper 51.

[7] Kim, V., "Main Physical Features and Processes Determining the Performance of Stationary Plasma Thrusters," *Journal of Propulsion Power*, Vol. 14, No. 7, 1998, pp. 736–743. doi:10.2514/2.5335

[8] Hofer, R. R., Jankovsky, R. S., and Gallimore, A. D., "High-Specific Impulse Hall Thrusters, Part 1: Influence of Current Density and Magnetic Field," *Journal of Propulsion Power*, Vol. 22, No. 4, 2006, pp. 721–731. doi:10.2514/1.15952

[9] Hofer, R. R., and Gallimore, A. D., "High-Specific Impulse Hall Thrusters, Part 2: Efficiency Analysis," *Journal of Propulsion Power*, Vol. 22, No. 4, 2006, pp. 732–740. doi:10.2514/1.15954

[10] Garrigues, L., Hagelaar, G. J. M., Bareilles, J., Boniface, C., and Boeuf, J. P., "Model Study of the Influence of the Magnetic Field Configuration on the Performance and Lifetime of a Hall Thruster," *Physics of Plasmas*, Vol. 10, No. 12, 2003, pp. 4886–4892. doi:10.1063/1.1622670

[11] Ahedo, E., and Escobar, D., "Influence of Design and Operation Parameters on Hall Thruster Performances," *Journal of Applied Physics*, Vol. 96, No. 2, 2004, pp. 983–992. doi:10.1063/1.1759790

[12] Gawron, D., Mazouffre, S., Sadeghi, N., and Héron, A., "Influence of Magnetic Field and Discharge Voltage on the Acceleration Layer Features in a Hall Effect Thruster," *Plasma Sources Science and Technology*, Vol. 17, No. 2, 2008, Paper 025001. doi:10.1088/0963-0252/17/2/025001

[13] Vilamot, R., "Optimisation de la Configuration Magnétique d'un Propulseur à Effet Hall par Résolution du Problème Magnétostatique Inverse," Ph.D. Thesis, Univ. de Toulouse, Toulouse, France, 2011 (in French).

[14] Henaux, C., Vilamot, R., Garrigues, L., and Harribey, D., "A New Flexible Magnetic Circuit for a Hall Effect Thruster," *Proceedings of 32nd International Electric Propulsion Conference*, IEPC Paper 11-291, Wiesbaden, Germany, 2011.

[15] Meeker, D., "Finite Element Method Magnetics User's Manual," Ver. 4.2, 2010, www.femm.info/wiki/HomePage.

[16] Garrigues, L., Mazouffre, S., Hénaux, C., Vilamot, R., Rossi, A., Harribey, D., Bourgeois, G., Vaudolon, J., and Zurbach, S., "Design and First Test Campaign Results with a New Flexible Magnetic Circuit for a Hall Thruster," *Proceedings of 33rd International Electric Propulsion Conference*, IEPC Paper 13-250, Washington, D.C., 2013.

[17] Brown, D. L., and Gallimore, A. D., "Evaluation of Facility Effects on Ion Migration in a Hall Thruster Plume," *Journal of Propulsion and Power*, Vol. 27, No. 3, 2011, pp. 573–585. doi:10.2514/1.B34068

[18] Walker, M. L. R., Hofer, R. R., and Gallimore, A. D., "Ion Collection in Hall Thruster Plumes," *Journal of Propulsion and Power*, Vol. 22, No. 1, 2006, pp. 205–209. doi:10.2514/1.11953

[19] Mikellides, I. G., Katz, I., Hofer, R. R., Goebel, D. M., and deGrys, K., "Magnetic Shielding of the Channel Walls in a Hall Plasma Accelerator," *Physics of Plasmas*, Vol. 18, No. 3, 2011, Paper 033501. doi:10.1063/1.3551583

[20] Mikellides, I. G., Katz, I., Hofer, R. R., and Goebel, D. M., "Magnetic Shielding of Walls from the Unmagnetized Ion Beam in a Hall Thruster," *Applied Physics Letters*, Vol. 102, No. 2, 2013, Paper 023509. doi:10.1063/1.4776192

[21] Goebel, D. M., Hofer, R. R., Mikellides, I. G., Katz, I., Polk, J. E., and Dotson, B., "Conducting Wall Hall Thrusters," *Proceedings of 33rd International Electric Propulsion Conference*, IEPC Paper 13-276, Washington, D.C., 2013, and references herein.

[22] Mazouffre, S., Vaudolon, J., Largeau, G., Hénaux, C., Rossi, A., and Harribey, D., "Visual Evidence of Magnetic Shielding with the PPS-Flex Hall Thruster," *Institute of Electrical and Electronics Engineers Transactions on Plasma Science*, Vol. 42, No. 10, 2014, pp. 2668–2669. doi:10.1109/TPS.2014.2331180

[23] Mazouffre, S., Tsikata, S., and Vaudolon, J., "Development and Experimental Characterization of a Wall-Less Hall Thruster," *Journal of Applied Physics*, Vol. 116, No. 24, 2014, Paper 243302. doi:10.1063/1.4904965

L. King
Associate Editor